

Comparing Treatments for Amblyopia with a Synaptic Plasticity Model

Brian S. Blais

Contents

Preface	1
Software Installation	2
1 Introduction	2
2 Methods	3
2.1 Natural Image Input Environment	3
2.2 Two-eye architecture	4
2.3 Synaptic Modification: The BCM Learning Rule	5
2.4 Simulation	8
2.5 Models of Development of Amblyopia	8
Refractive amblyopia	10
Strabismic amblyopia	10
2.6 Models of Treatments for Amblyopia	12
Optical Fix	12
Patch treatment	12
Contrast modification	12
Atropine treatment	13
Dichoptic Masks	13
2.7 Quantifying responses	14
Ocular Dominance Index	14
3 Results	14
3.1 Refractory and Strabismic Amblyopia	14
3.2 Treatments	18
Optical Fix	18
Patch Treatment	18
Atropine Treatment	18
3.3 Contrast and Mask	18
4 Conclusions and Discussion	23
Some lingering questions	24
References	24

Preface

These notes are produced with a combination of Obsidian (<https://obsidian.md>), pandoc (<https://pandoc.org>), and some self-styled python scripts (<https://github.com/bblais/Amblyopia-Simulation/tree/main/Manuscript>)

Software Installation

The software is Python-based with parts written in Cython.

- Download the Anaconda Distribution of Python:

<https://www.anaconda.com/products/individual#downloads>

- Download and extract the *PlasticNet* package at:

<https://github.com/bblais/Plasticnet/archive/refs/heads/master.zip>

- Run the script `install.py`

1 Introduction

Amblyopia is the most common cause of vision loss in children, caused by refractive errors or misalignment of the eyes (Zárate and Tejedor, 2007). It is associated with deficits in many aspects of vision including visual acuity, contrast sensitivity, color, depth (stereopsis), and motion(Birch, 2013). The current primary treatments are described in the *Amblyopia Preferred Practice Method* (Wallace et al., 2018). These treatments are divided into two broad categories, monocular and binocular treatments.

Monocular treatments produce a competition between the two eyes by treating only the fellow eye so that the amblyopic eye recovers. The most common treatment includes the optical correction of significant refractive errors followed by patching the dominant eye which forces the visual input to come from only the amblyopic eye. Although patching is the most common method of treatment, other methods include including pharmacology and technology (Gao et al., 2018; Glaser et al., 2002; Jonathan M. Holmes et al., 2016b; Jonathan M. Holmes et al., 2016a; Kelly et al., 2016; Li et al., 2015; Zárate and Tejedor, 2007). One such pharmacological treatment is the application of atropine drops in the fellow eye, resulting in a decreased efficacy of visual inputs through the fellow eye. Each of the monocular treatments applies only to the fellow eye and the amblyopic eye is left untouched.

Binocular treatments seek to stimulate both eyes in such a way that binocular mechanisms can produce a recovery in the amblyopic eye[Hess and Thompson (2015); holmes2016randomized]. The binocular treatment that we will be addressing here uses virtual reality headsets(Xiao et al., 2020, 2022) to provide input to both eyes, with contrast modification and/or dichoptic masks presented independently to the amblyopic eye and the fellow eye. Although we focus on this particular form of binocular treatment, our approach applies equally well to any proposed treatment protocol.

Since the unequal visual input to the brain can cause alterations in the synaptic pathways leading to a disparity in ocular dominance (Birch, 2013), it is important to understand the possible synaptic effects amblyopia can produce and how potential treatments will either help or hinder the recovery. This work is an exploration of the problem of modeling amblyopia and its various treatments using synaptic plasticity models. The process involves constructing a simplified mechanism for the development of amblyopic deficits and subsequently modeling both monocular and binocular treatment protocols. The goal is to understand the dynamics of the recovery from

amblyopic deficits for the different treatment protocols, to compare the effectiveness of each protocol, and to explore their limitations. Ideally we would like to use these models to inform future protocol parameters and perhaps suggest novel treatments for amblyopia.

2 Methods

In this paper we use a specific model of neural plasticity, the BCM model(Bienenstock et al., 1982), to describe the dynamics of the recovery from amblyopia under a number of treatment protocols.

2.1 Natural Image Input Environment

We use natural scene stimuli for the simulated inputs to the visual system. We start with images taken with a digital camera, with dimensions 1200 pixels by 1600 pixels scaled down to 600 pixels by 800 pixels (Figure 1). Given the scale invariance of natural images(Ruderman and Bialek, 1994), angular sizes of images are not useful in establishing the connection between image pixels and angular measurements. We thus turn to the literature on the properties of cells in the retinal-LGN-V1 pathway to establish this connection.

The size of LGN receptive fields (RF) and V1 receptive fields are approximately 3° (DeAngelis et al., 1995) and 5° - 8° .[DeAngelis et al. (1995); van2010receptive], respectively. We use a Difference-of-Gaussians (DOG) filter to model the center-surround retinal/LGN processing using filter sizes $\sigma_s = 1\text{pix}$ and $\sigma_s = 3\text{pix}$ for the center and surround, respectively. Comparing the LGN RF size (3°) to a 2σ radius of the Difference-of-Gaussians (DOG) filter we get an approximate conversion between images pixels and real-world angular sizes,

$$\begin{aligned} 2\sigma_s &\equiv r_{\text{surround}} \\ 2r_{\text{surround}} &= 3^\circ = 4\sigma_s = 12\text{pix} \\ 1\text{pix} &= 0.25^\circ \end{aligned}$$

Using $1\text{pix} = 0.25^\circ$ as the conversion we then arrive at the V1 RF size: $5^\circ = 20\text{pix}$. For computational convenience we use a $19\text{pix} \times 19\text{pix}$ RF size for our simulations of the V1 cells, but the results are robust to receptive field size.

The early visual system computes different versions of response normalization, including the light adaptation of photoreceptors so their responses reflect *contrast* (i.e. difference from the mean) rather than intensity directly which allows the photoreceptors to respond to a wide range of intensities (Carandini and Heeger, 2012). We will be using mean-zero inputs for simplicity, this light adaptation is the same as the following,

$$R = (I - I_m)/I_\sigma$$

where I is the light intensity, I_m is the average light intensity (i.e. background intensity) and I_σ is the standard deviation of the light intensity (i.e. background variation). For small contrast, the response R scales as the intensity.

Ganglion cells add another normalization step, a contrast normalization effect of a suppressive field(Carandini and Heeger, 2012). This is approximately the same as the response normalization above, applied to the result of a center-surround ganglion response profile.

To model visual responses, we start with raw grayscale images, whose values range from 0 to 255. We first apply any external filtering (e.g. optical fix, refractive errors, patch treatments, etc...) to the images, and then apply the photoreceptor light adaptation and the ganglion contrast normalization. We model the ganglion response profile using a 32x32 pixel center-surround difference-of-Gaussians (DOG) filter to process the images. The center-surround radius ratio used for the ganglion cell is 1:3, with balanced excitatory and inhibitory regions and normalized Gaussian profiles. To simplify the number of parameters, the suppressive field is taken to much larger than the surround field of the ganglion cell response so we can approximate the ganglion cell contrast normalization with a simple numerical normalization across the ganglion responses(B. S. Blais et al., 1998). The resulting processed images are shown in Figure 2.



Figure 1: Original natural images.

2.2 Two-eye architecture

Shown in Figure 3 is the visual field, approximated here as a two-dimensional projection, to left and right retinal cells. These left and right retinal cells project to the left- and right-LGN cells, respectively, and finally to a single cortical cell. The retinal-LGN pathway is assumed to result in a center-surround filtering of the input patterns, as described in Section 2.1. It is important to understand that the model we are pursuing here is a *single cortical cell* which receives input from both eyes. We will encounter some limitations to this model which may necessitate exploring multi-neuron systems or a multi-cortical-layer architecture.

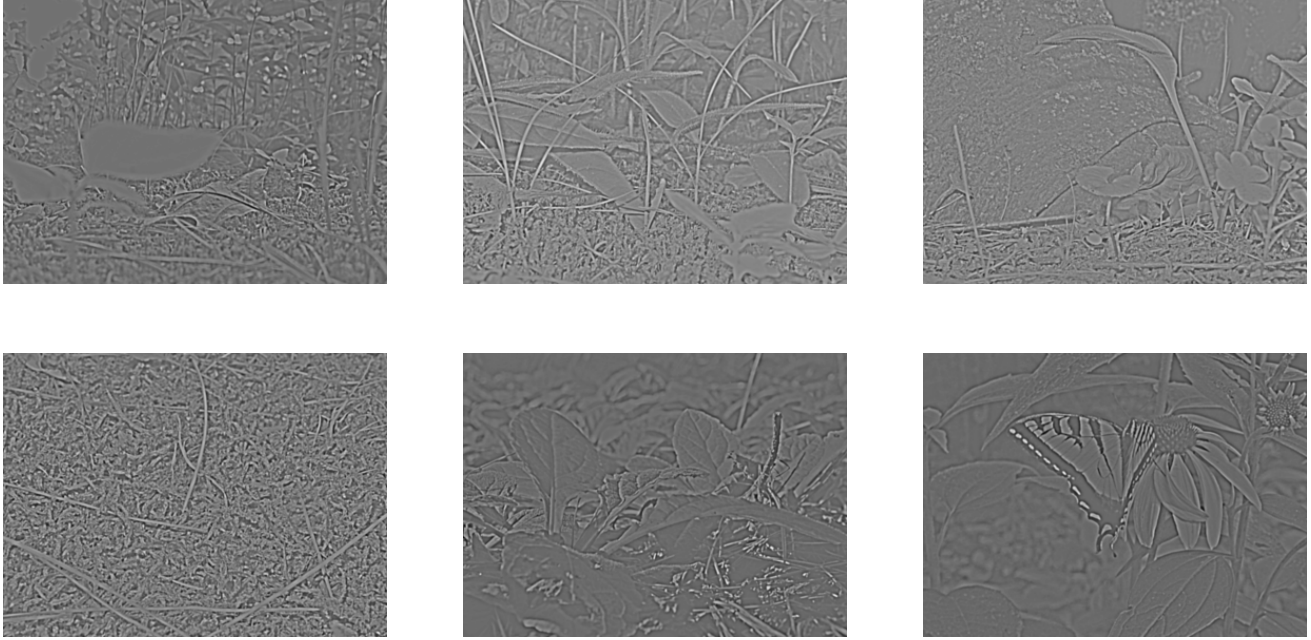


Figure 2: A small subset of the natural images filtered with light adaptation from the photoreceptors and the contrast normalization from the center-surround profile of the ganglion/LGN cells. Thus the images represent high LGN activity as white and low LGN activity as dark.

In the model, normal development is simulated with image patches presented to both eyes. These patches are taken from the same image at a time, and differ between the eyes in two possible ways: jitter and noise. What we are calling *jitter* is the difference in location between the patches between the eyes, specified by two parameters: μ_c which is the mean pixel difference between the patches and σ_c is the standard deviation of the pixel differences across many presentations. For example, if $\mu_c = 0$ and $\sigma_c = 0$ then the patches presented to each eye would be identical and if $\mu_c = 3$ and $\sigma_c = 0$ then every set of image patches presented would be separated by 3 pixels every time, etc... What we are calling *noise* is random variation of each input generated from a zero-mean normal distribution of a particular variance, representing the natural variation in responses of LGN neurons. Practically, the independent random noise added to each of the two-eye channels avoids the artificial situation of having mathematically identical inputs in the channels. The development of the deficit and the subsequent treatment protocols are modeled with added preprocessing to these image patches, described later in Sections 2.5 and 2.6.

For all of the simulations we use a 19x19 receptive field, which is a compromise between speed of simulation and the limits of spatial discretization. We perform at least 20 independent simulations for each condition to address variation in the results.

2.3 Synaptic Modification: The BCM Learning Rule

We use a single neuron and the parabolic form of the BCM(Bienenstock et al., 1982; Brian S. Blais et al., 2008) learning rule for all of the simulations, where the synaptic modification depends on the postsynaptic activity, y , in the following way for a single neuron

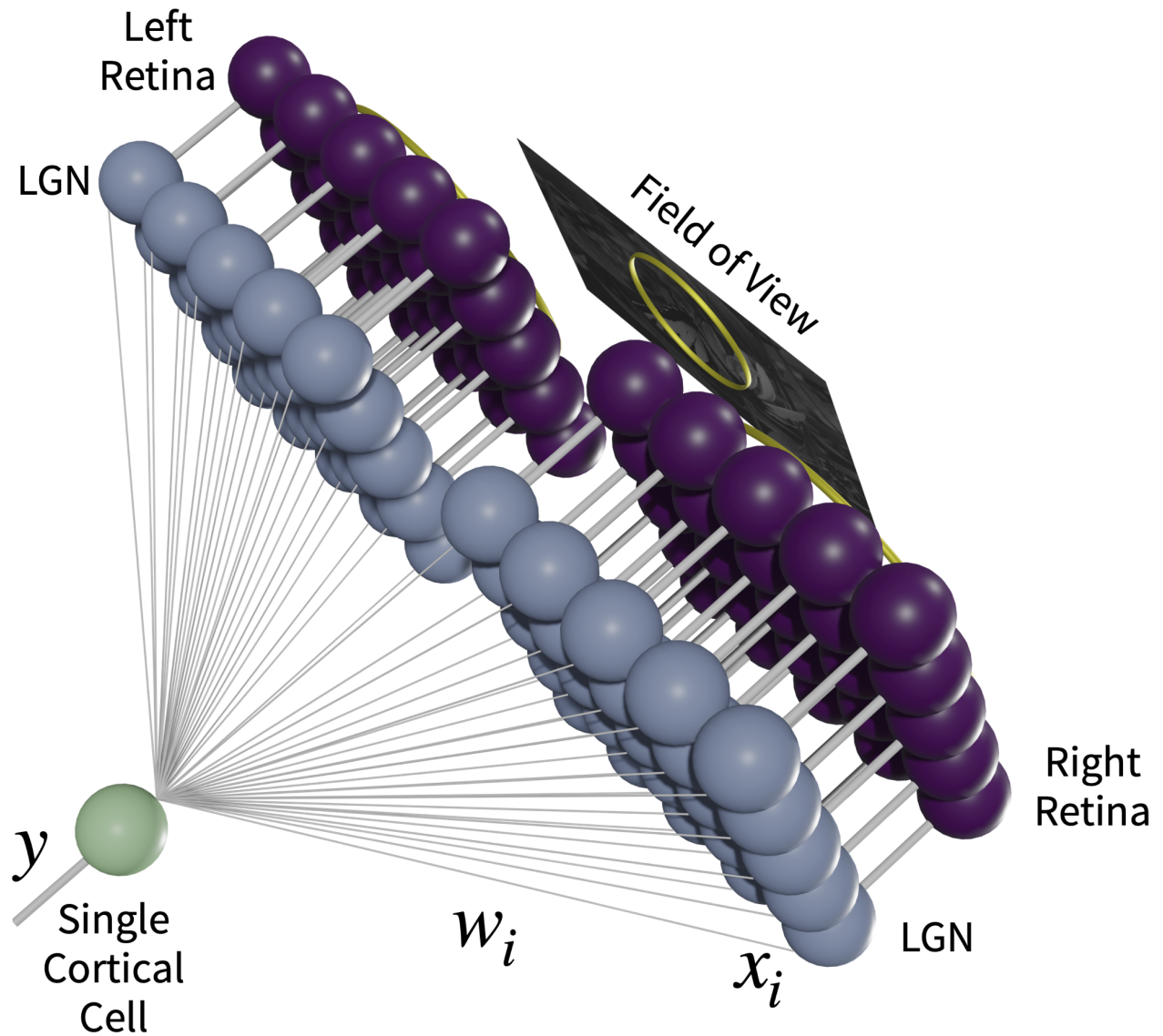
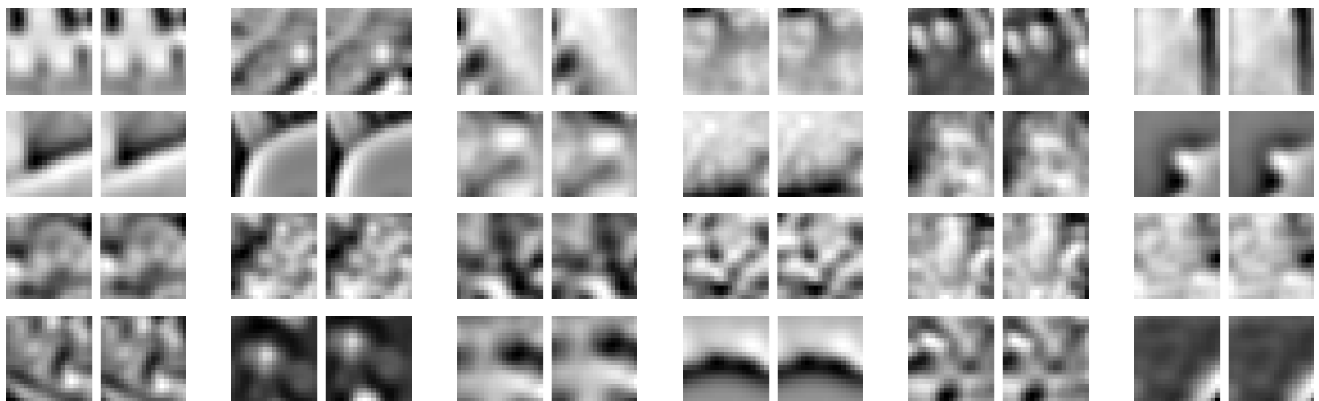


Figure 3: Two-eye architecture.

Figure 4: A sample of 24 input patches from a normal visual environment with jitter parameters $\mu_c = 0$ and $\sigma_c = 0$. The left- and right-eye inputs are shown in pairs.

$$y = \sigma \left(\sum_i x_i w_i \right)$$

$$\frac{dw_i}{dt} = \eta y (y - \theta_M) x_i$$

$$\frac{d\theta_M}{dt} = (y^2 - \theta_M)/\tau$$

where x_i is the i th presynaptic input, w_i is the i th synaptic weight, and y is the postsynaptic output activity. The constant, η , refers to the learning rate and the constant, τ , is what we call the memory-constant and is related to the speed of the sliding threshold. The transfer function, $\sigma(\cdot)$, places minimum and maximum responses given a set of inputs and weights.

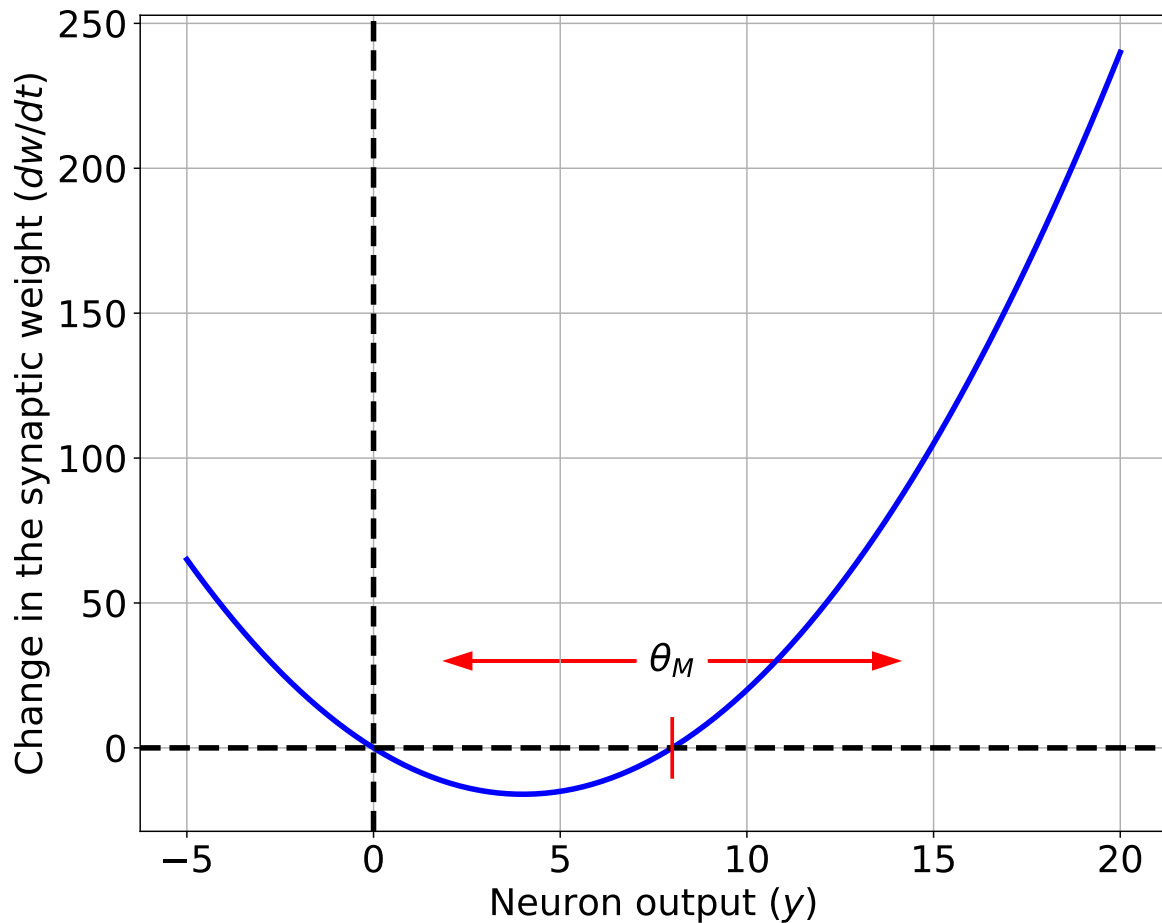


Figure 5: The BCM synaptic modification function. Units are arbitrary.

The results are extremely robust to values of η and τ , which are generally chosen for practical, rather than theoretical, considerations. Each of these constants is related to the time-step for the simulations, but given the

phenomenological nature of the BCM theory it is beyond the scope of this paper to make detailed comparisons between simulation time and real-time. Further, the fact that τ can be changed within a factor of 100 with no noticeable effect, the experiments presented here cannot be used address the time-scales of the molecular mechanisms underlying synaptic modification. Whenever we refer to real-time units for a simulation, we approximate a single simulation iteration as 1 iteration = 0.2 seconds(Brian S. Blais, 1998).

In the BCM learning rule, weights decrease if y is less than the modification threshold, θ_M , and increase if y is greater than the modification threshold. To stabilize learning, the modification threshold “slides” as a super-linear function of the output. The output, y , is related to the product of the inputs and the weights via a sigmoidal function, $\sigma(\cdot)$, which places constraints on the values of the output, keeping it in the range -1 and 50. The interpretation of negative values is consistent with previous work(B. S. Blais et al., 1998), where the activity values are measured relative to spontaneous activity. Thus, negative values are interpreted as activity below spontaneous. We continue this usage, in order to more easily compare with previous simulations. The role of the spontaneous level for the simulations in the natural image environment is discussed elsewhere(B. S. Blais et al., 1998).

2.4 Simulation

The synaptic weights, and the modification threshold, are set to small random initial values at the beginning of a simulation. At each iteration, an input patch is generated as described above depending on the procedure being simulated and then presented to the neuron. After each input patch is presented, the weights are modified using the output of the neuron, the input values and the current value of the modification threshold. In an input environment composed of patches taken from natural images, with equal patches presented to the left- and right-eyes as shown in Figure 4, this process orientation selective and fully binocular cells(B. S. Blais et al., 1998). We then present test stimulus made from sine-gratings with 24 orientations, 20 spatial frequencies, and optimized over phase. Applying any of the blur filters to the sine gratings does not quantitatively change the result.

2.5 Models of Development of Amblyopia

Amblyopia is a reduction of the best-corrected visual acuity (BCVA) with an otherwise normal eye and has many causes(Wallace et al., 2018). Two of the most common forms of amblyopia are strabismic and anisometropic amblyopia. Strabismic amblyopia occurs when the inputs from each eye do not converge and the fixating eye becomes dominant over a non-fixating eye. Refractive amblyopia occurs with untreated unilateral refractive errors, one kind being anisometropic amblyopia where unequal refractive power in each eye leads the retinal image from the amblyopic eye to be blurred relative to the fellow eye. Both of these processes lead to synaptic plasticity adjustments and interocular competition, enhancing the initial deficit.

In this work we use a model of the amblyopic deficit caused by two mechanisms. The first is a blurring of the amblyopic eye inputs, representing refractive amblyopia. The second is eye-jitter, representing one source of strabismic amblyopia(Charters and Ghasia, 2022). We have used the approximate values of $\mu_c = 7.5$ and $\sigma_c = 2$ to represent significant strabismus – nearly half of a receptive field offset with a strong variation on the order of

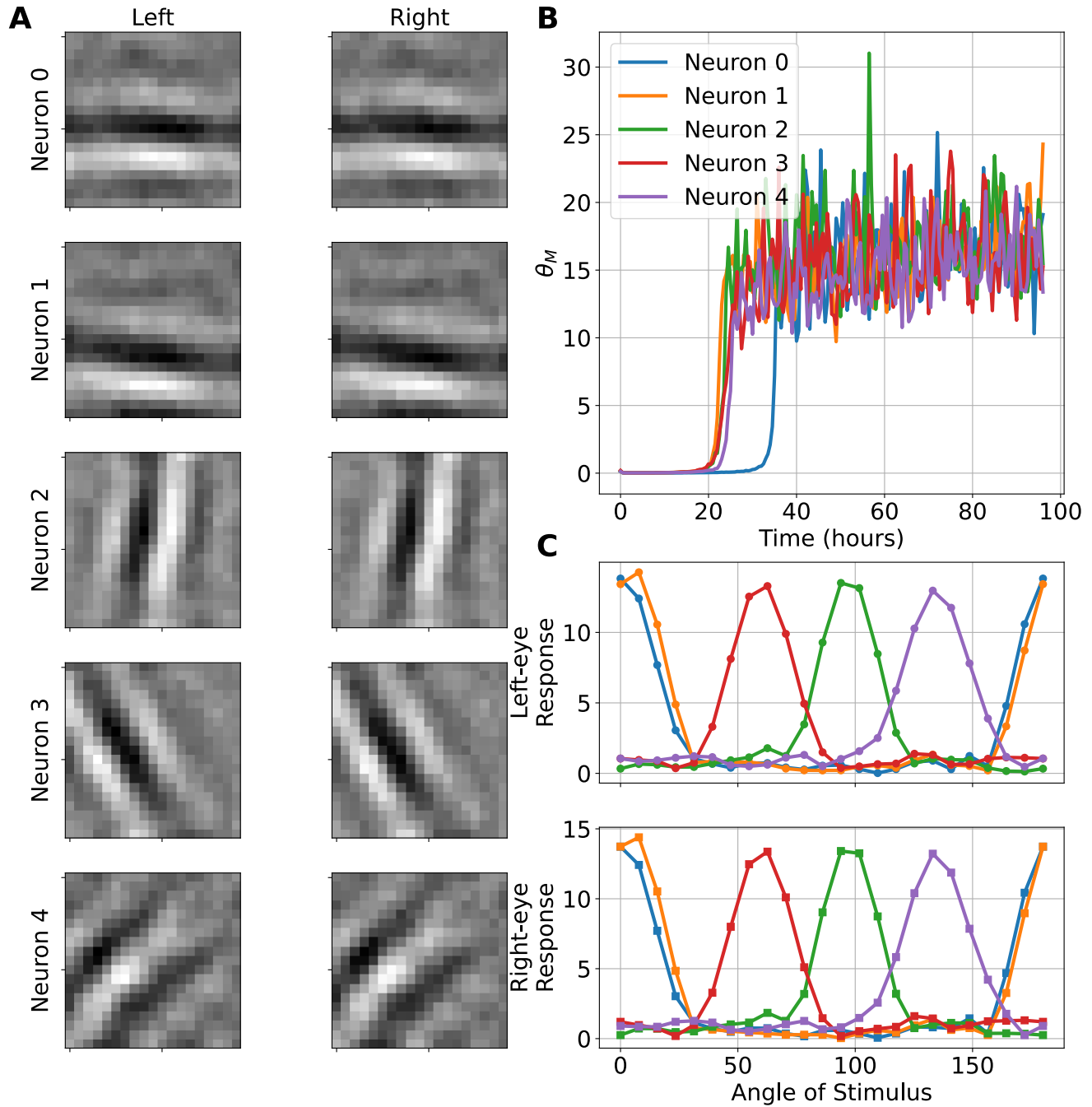


Figure 6: (A) Synaptic weights where black denotes weak weights and white denotes strong weights. A clear preference for oriented stimuli can be seen. (B) BCM modification threshold over time. The value converges to nearly the same level for all neurons. (C) Responses to Oriented Stimuli after training. Each neuron develops orientation selectivity to a range of optimum angles.

25% of the RF size. We can explore these mechanisms independently and in conjunction to see how they respond differentially to the various treatments.

Refractive amblyopia

The amblyopic eye is presented with image patches that have been *blurred* with a normalized Gaussian filter applied to the images with a specified width. The larger the width the blurrier the resulting filtered image. Some examples are shown in Figure 7

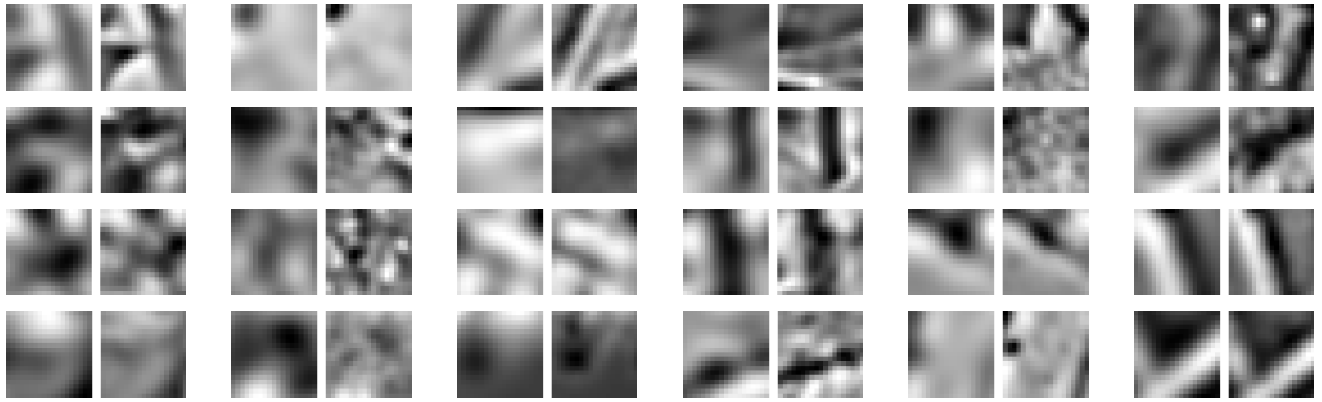


Figure 7: A sample of 24 input patches from a refractive amblyopic environment. The amblyopic (blurred) input is the square on the left-hand side of each pair.

Strabismic amblyopia

Strabismic inputs are modeled by changing the center of the left- and right-input patches in a systematic way, with a set mean offset (μ_c) and a standard deviation (σ_c) per input patch generated. In this way we can model completely overlapping ($\mu_c = 0$) inputs, completely non-overlapping (i.e. extreme strabismus, $\mu_c > 19$), and any amount of overlap in between. Some examples are shown in Figure 8 with the offset locations shown in Figure 9.



Figure 8: A sample of 24 input patches from a strabismic visual environment achieved through random jitter between the amblyopic (left) eye and the fellow (right) eye.

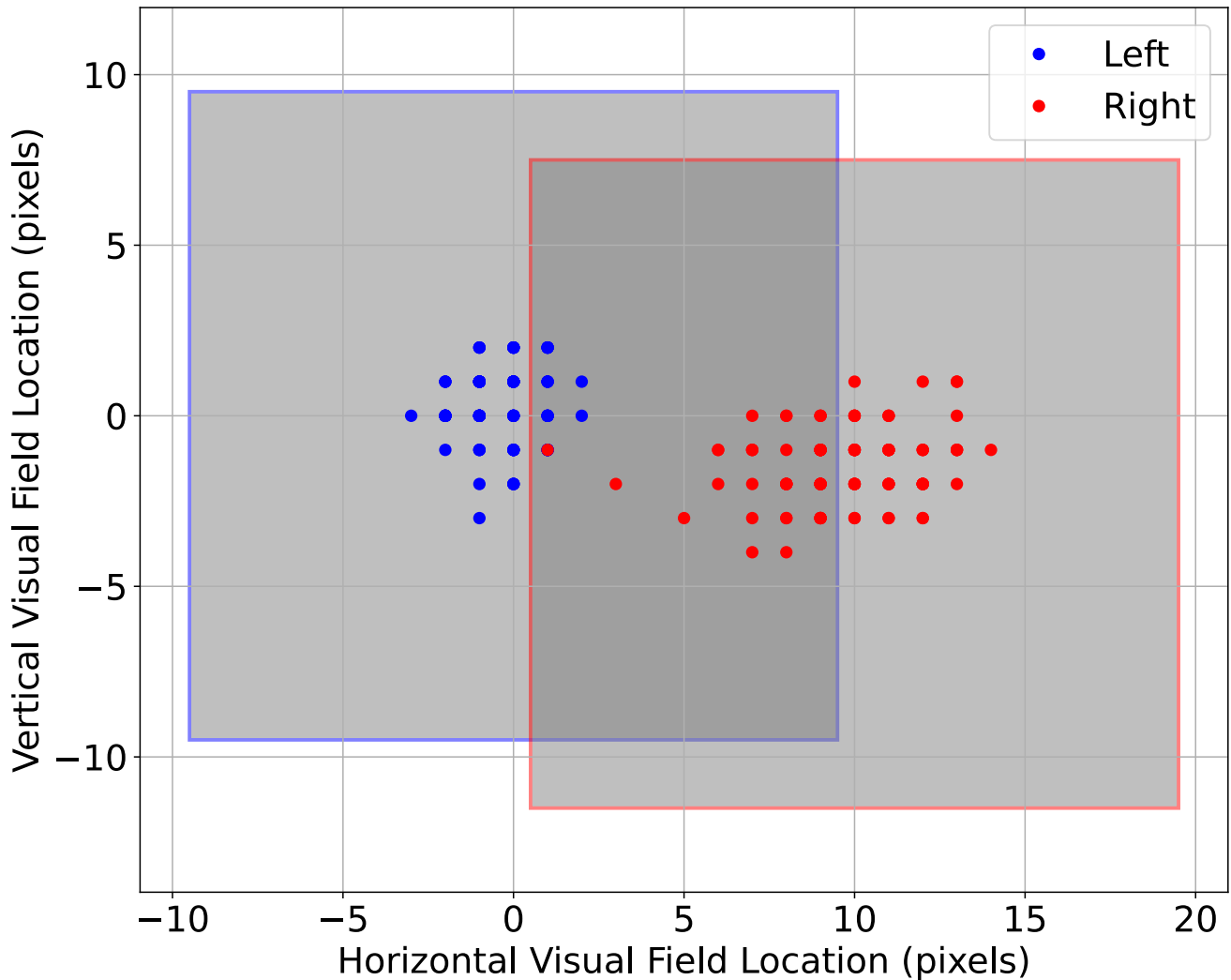


Figure 9: Locations of the center of the left- and right-field of view receptive fields, jittered randomly with set mean and standard deviation. The average receptive fields are shown as gray squares.

2.6 Models of Treatments for Amblyopia

Optical Fix

To model the fix to the refractive imbalance we follow the deficit simulation described above with an input environment that is rebalanced. Both eyes receiving nearly identical input patches (4) without any blur filter on the amblyopic eye but with the same jitter and noise deviations as described above. This process is a model of the application of refractive correction.

Patch treatment

The typical patch treatment is done by depriving the fellow-eye of input with an eye-patch. In the model this is equivalent to presenting the fellow-eye (taken to be the right-eye in the simulations) with random noise instead of the natural image input. Competition between the left- and right-channels drives the recovery, and is produced from the difference between *structured* input into the amblyopic-eye and the *unstructured* (i.e. noise) input into the fellow eye. It is not driven by a reduction in input activity. 10 shows sample simulation input patterns from the patched eye. Compare this to 4 to see that the simulated patch has far less structure than the normal inputs.

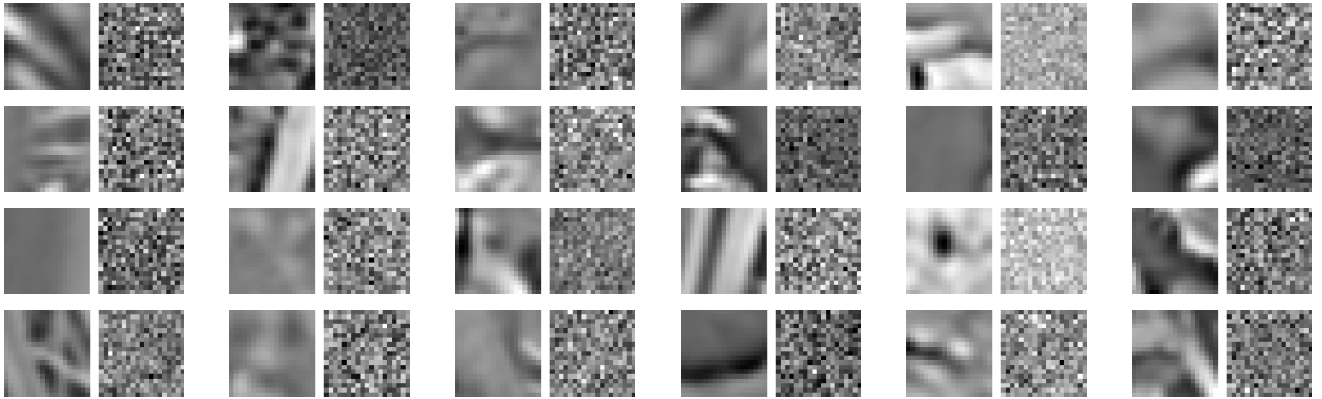


Figure 10: A sample of 24 input patches from a patched visual environment. Shown is the input to the amblyopic eye (left) which is the normal visual environment and the input to the fellow eye (right) which consists of random noise.

Contrast modification

A binocular approach to treatment can be produced with contrast reduction of the non-deprived channel relative to the deprived channel. Experimentally this can be accomplished with VR headsets(Xiao et al., 2020). In the model we implement this by down-scaling the fellow-eye channel with a simple scalar multiplier applied to each pixel. The contrast difference sets up competition between the two channels with the advantage given to the amblyopic-eye channel.

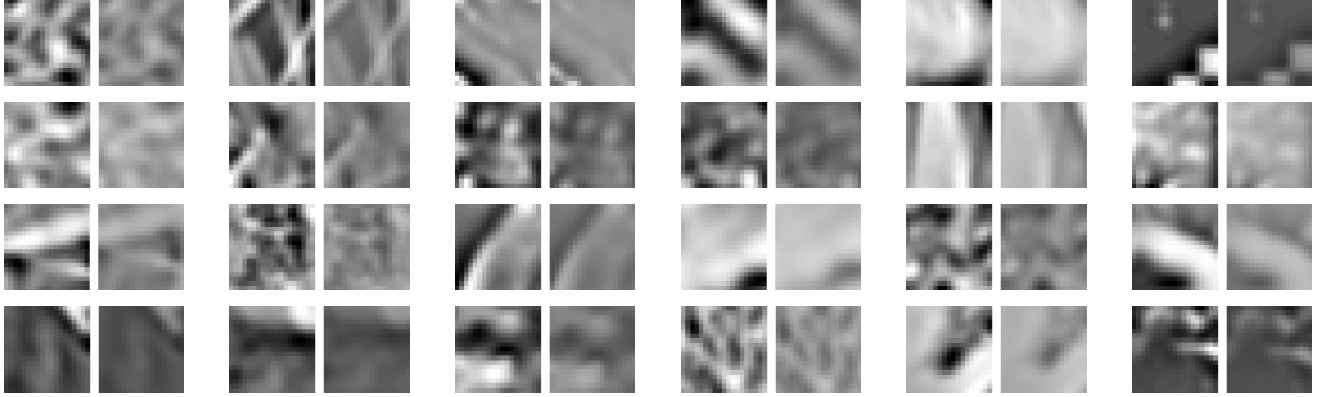


Figure 11: A sample of 24 input patches from a contrast modified visual environment. Shown is the input to the amblyopic eye (left) which is the normal visual environment and the input to the fellow eye (right) which is the same input but with contrast reduced.

Atropine treatment

In the atropine treatment for amblyopia(Glaser et al., 2002), eye-drops of atropine are applied to the fellow-eye resulting in blurred vision in that eye. Here we use the same blurred filter used to obtain the deficit (possibly with a different width) applied to the fellow eye (Figure 12). The difference in sharpness between the fellow-eye inputs and the amblyopic-eye inputs sets up competition between the two channels with the advantage given to the amblyopic-eye.

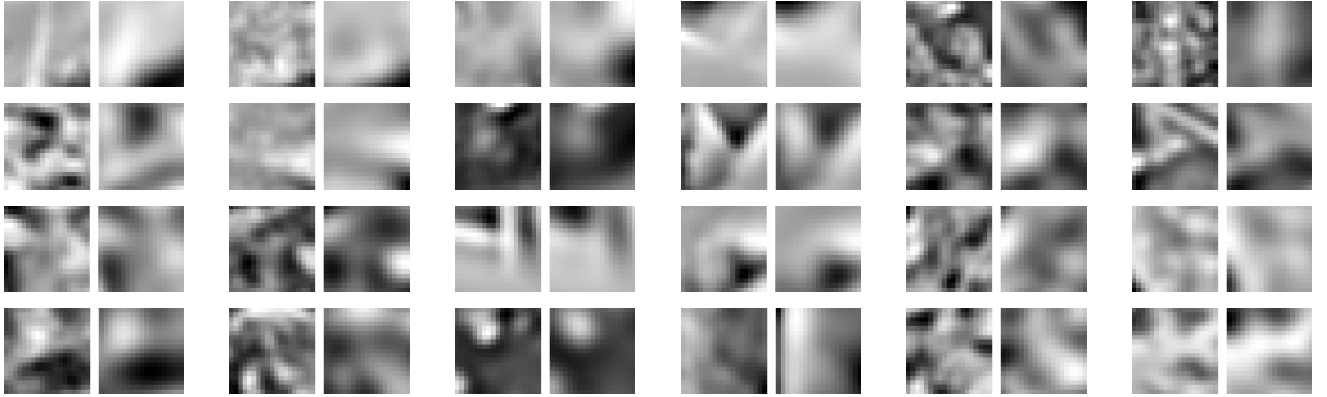


Figure 12: A sample of 24 input patches from a simulated atropine treatment environment. Shown is the input to the amblyopic eye (left) which is the normal visual environment and the input to the fellow eye (right) which is the same input but blurred with a Gaussian filter.

Dichoptic Masks

On top of the contrast modification, we can include the application of the dichoptic mask. In this method, each eye receives a version of the input images filtered through independent masks in each channel, resulting in a mostly-independent pattern in each channel. It has been observed that contrast modification combined with dichoptic masks can be an effective treatment for amblyopiaXiao et al. (2022). The motivation behind the application of the

mask filter is that the neural system must use both channels to reconstruct the full image and thus may lead to enhanced recovery.

The dichoptic masks are constructed with the following procedure. A blank image (i.e. all zeros) is made to which is added 15 randomly sized circles with values equal to 1 (Figure 13 A). These images are then smoothed with a Gaussian filter of a given width, f (Figure 13 B). This width is a parameter we can vary to change the overlap between the left- and right-eye images. A high value of f compared with the size of the receptive field, e.g. $f = 90$, yields a high overlap between the patterns in the amblyopic- and fellow-eye inputs (Figure 14). Likewise, a small value of f , e.g. $f = 10$, the eye inputs are nearly independent – the patterned activity falling mostly on one of the eyes and not much to both. Finally, the smoothed images are scaled to have values from a minimum of 0 to a maximum of 1. This image-mask we will call A , and is the left-eye mask whereas the right-eye mask, F , is the inverse of the left-eye mask, $F \equiv 1 - A$. The mask is applied to an image by multiplying the left- and right-eye images by the left- and right-eye masks, respectively, resulting in a pair of images which have no overlap at the peaks of each mask, and nearly equal overlap in the areas of the images where the masks are near 0.5 (Figure 15).

2.7 Quantifying responses

Ocular Dominance Index

Simulations are ended when selectivity has been achieved and the responses are stable. From the maximal responses of each eye, R_{left} and R_{right} , individually, we can calculate the ocular dominance index as

$$\text{ODI} \equiv \frac{R_{\text{right}} - R_{\text{left}}}{R_{\text{right}} + R_{\text{left}}}$$

The ocular dominance index (ODI) has a value of $\text{ODI} \approx 1$ when stimulus to the right-eye (typically the fellow eye in the simulations, by convention) yields a maximum neuronal response with little or no contribution from the left-eye. Likewise, an ocular dominance index (ODI) has a value of $\text{ODI} \approx -1$ when stimulus to the left-eye (typically the amblyopic eye, by convention) yields a maximum neuronal response with little or no contribution from the right-eye. A value of $\text{ODI} \approx 0$ represents a purely binocular cell, responding equally to stimulus in either eye.

3 Results

3.1 Refractory and Strabismic Amblyopia

Figure 16 shows the production of a deficit effect using both refractory blurring and inter-eye jitter. The refractory blur has a much larger effect, with larger blur resulting in a more pronounced deficit. For the sake of convenience, we use a blur=4 for the rest of the simulations because it gives a robust deficit effect without being overwhelming.

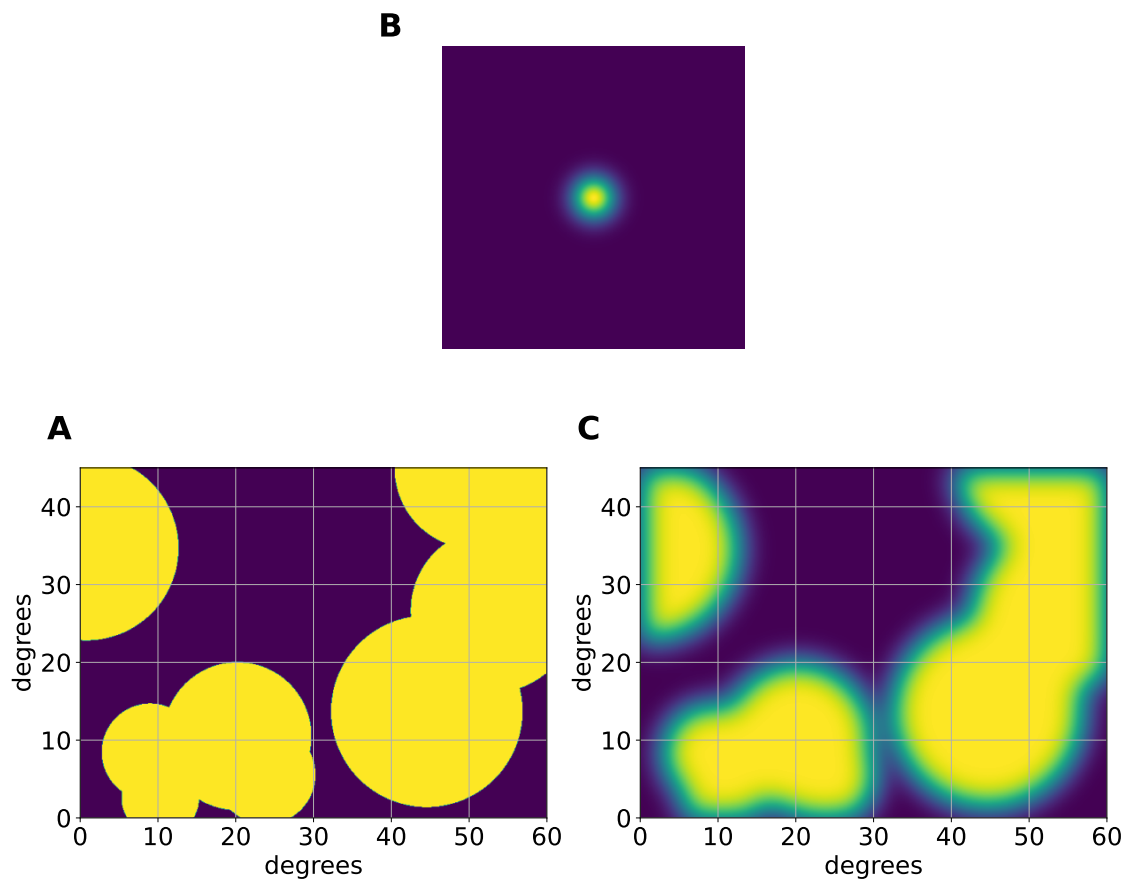


Figure 13: The dichoptic masks are produced by taking random circular blobs (A), convolving them a Gaussian filter of a specified size (B), resulting in the circular blobs blending into the background smoothly at the edges on the scale of the filter (C)

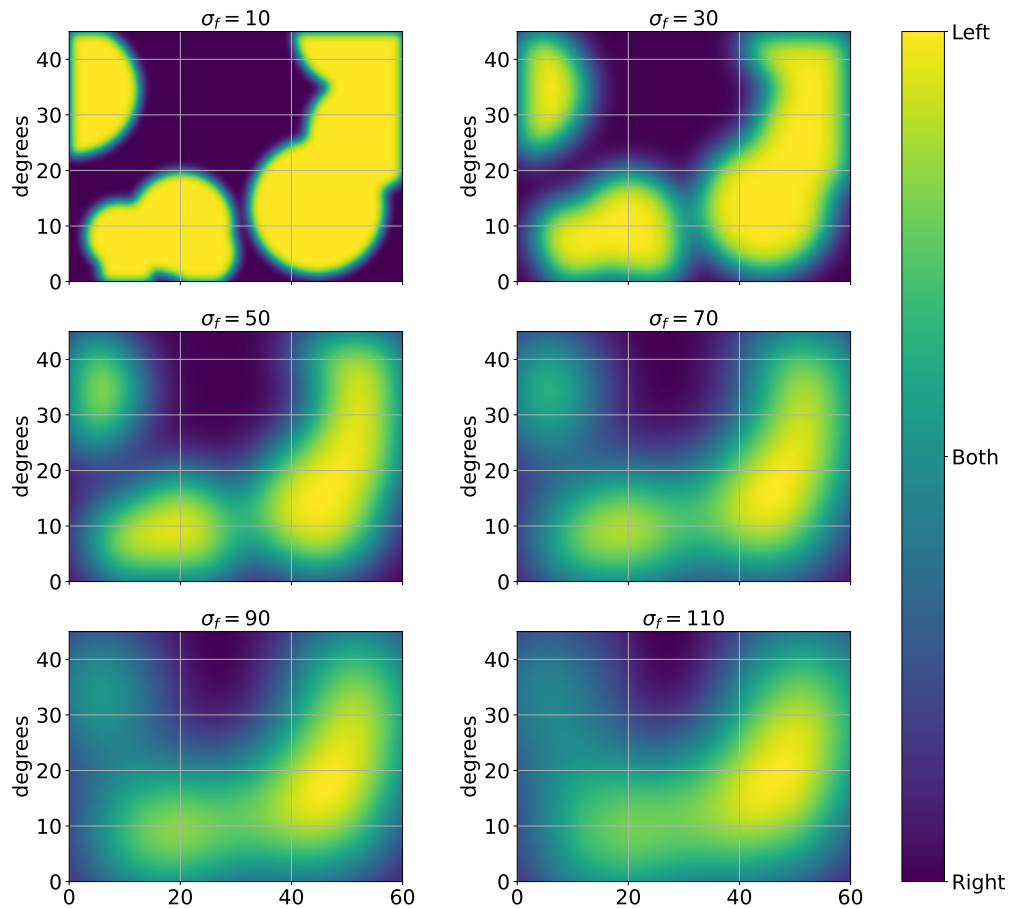


Figure 14: The dichoptic masks for several different filter sizes. The larger the filter, the larger the overlap in the patterns presented to the two eyes. For a very sharp mask (upper left) patterns are nearly all to either the left or the right eye. For a wide mask (lower right) most patterns are presented to both eyes.

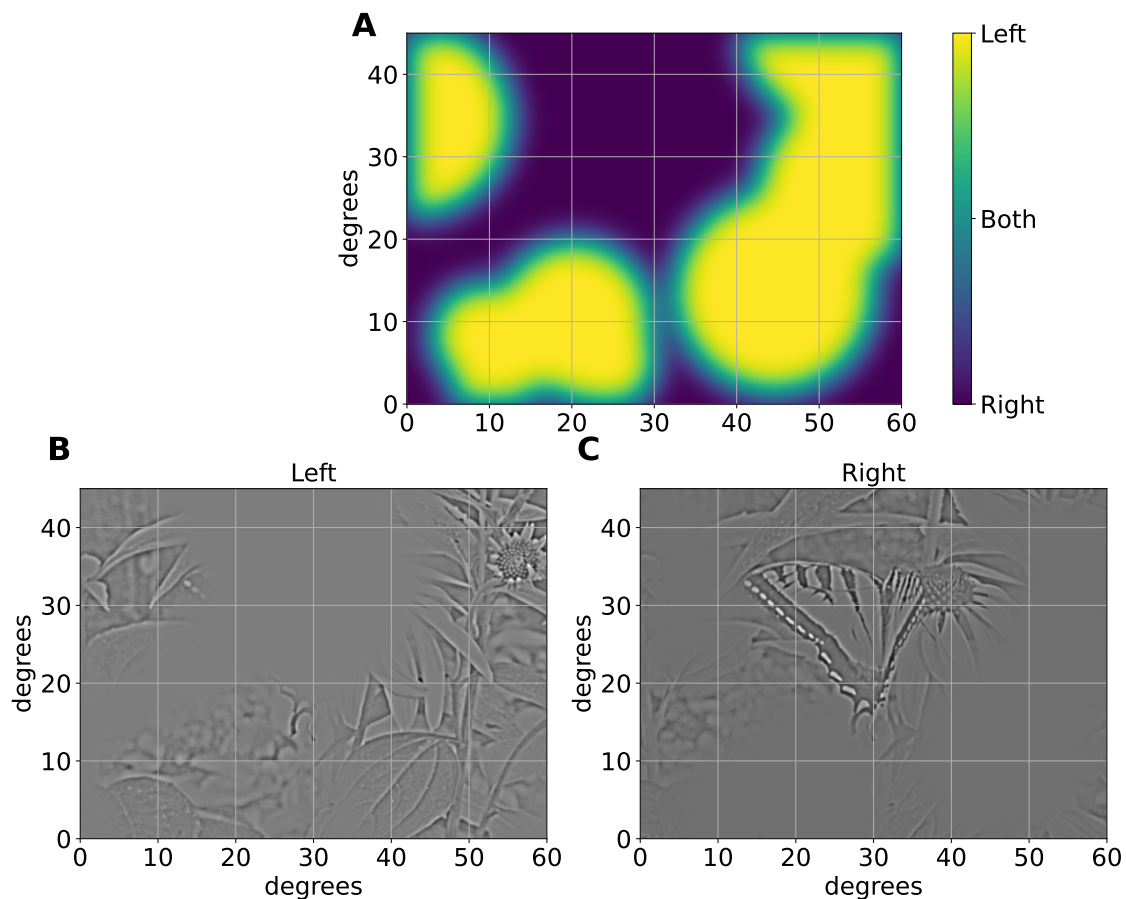


Figure 15: An example of a dichoptic mask, $\sigma_f = 20$, applied to one of the images. The mask (A) shows how much of the input goes to each of the left and right channels. The resulting left- and right-images (B and C, respectively) show the results of the partial independence of the two channels. One can see areas where there is some overlap as well as areas where the pattern is only present in one of the eyes due to the application of the mask.

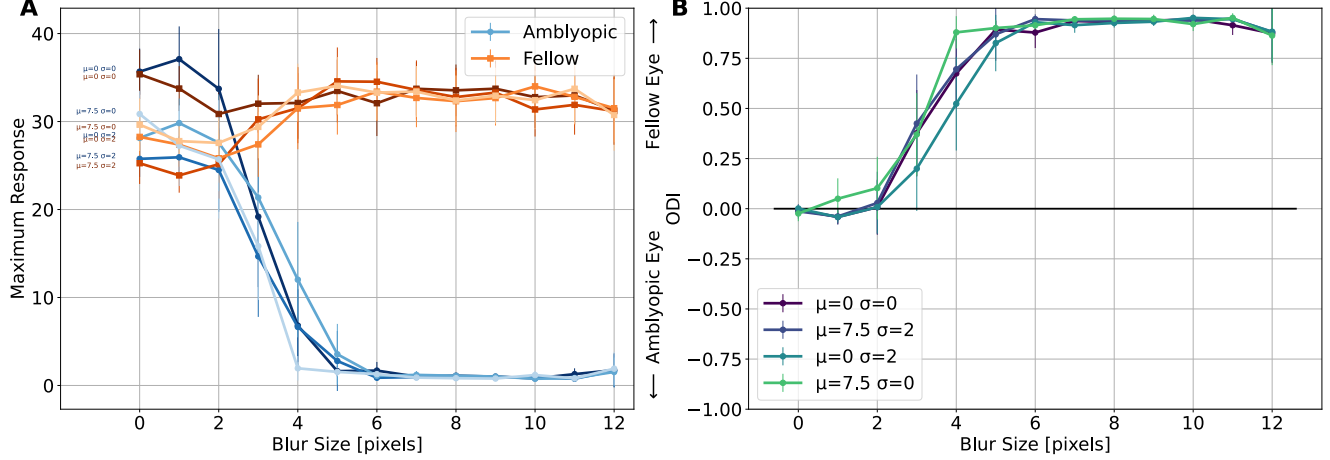


Figure 16: Deficit maximum response for the amblyopic- and fellow-input channels (A) and the resulting ODI (B) as a function of the deficit blur size (in pixels) with several combinations of the jitter offset mean (μ_c) standard deviation (σ_c). Interestingly, the jitter does very little other than make the variation higher.

3.2 Treatments

Optical Fix

Shown in Figure 17 are the results for the optical fix as a function of the open-eye noise. For larger open-eye noise, the recovery rate (Figure 17 C) increases. Changing jitter increases the variability and seems to increase the effectiveness of the treatment, at least for low-noise, but the results are not statistically significant.

Patch Treatment

Shown in Figure 18 are the results for the patch treatment as a function of the closed-eye noise. For larger closed-eye noise, the recovery rate (Figure 18 C) increases – up to a high level of noise, where it tapers off. Changing jitter increases the variability and seems to increase the effectiveness of the treatment – especially for the mean value of the jitter. Above a noise level of 0.5 the variability becomes so large that no further recovery can be seen.

It is surprising that we don't get a reverse amblyopia effect for large noise, but it may be masked by the increased variability.

Atropine Treatment

Shown in Figure 19 are the results for the atropine treatment as a function of the blur size. For larger blur size, the recovery rate (Figure 18 C) increases and saturates at a point lower than that for patch treatment. As for the other treatments, changing jitter increases the variability but has little other effect.

3.3 Contrast and Mask

Figure 20 shows the effect of contrast and dichoptic masks for the case of no eye-jitter while Figure 21 shows the same for a large eye-jitter. The mask enhances the rate of recovery for small contrasts (contrast<0.4), and doesn't

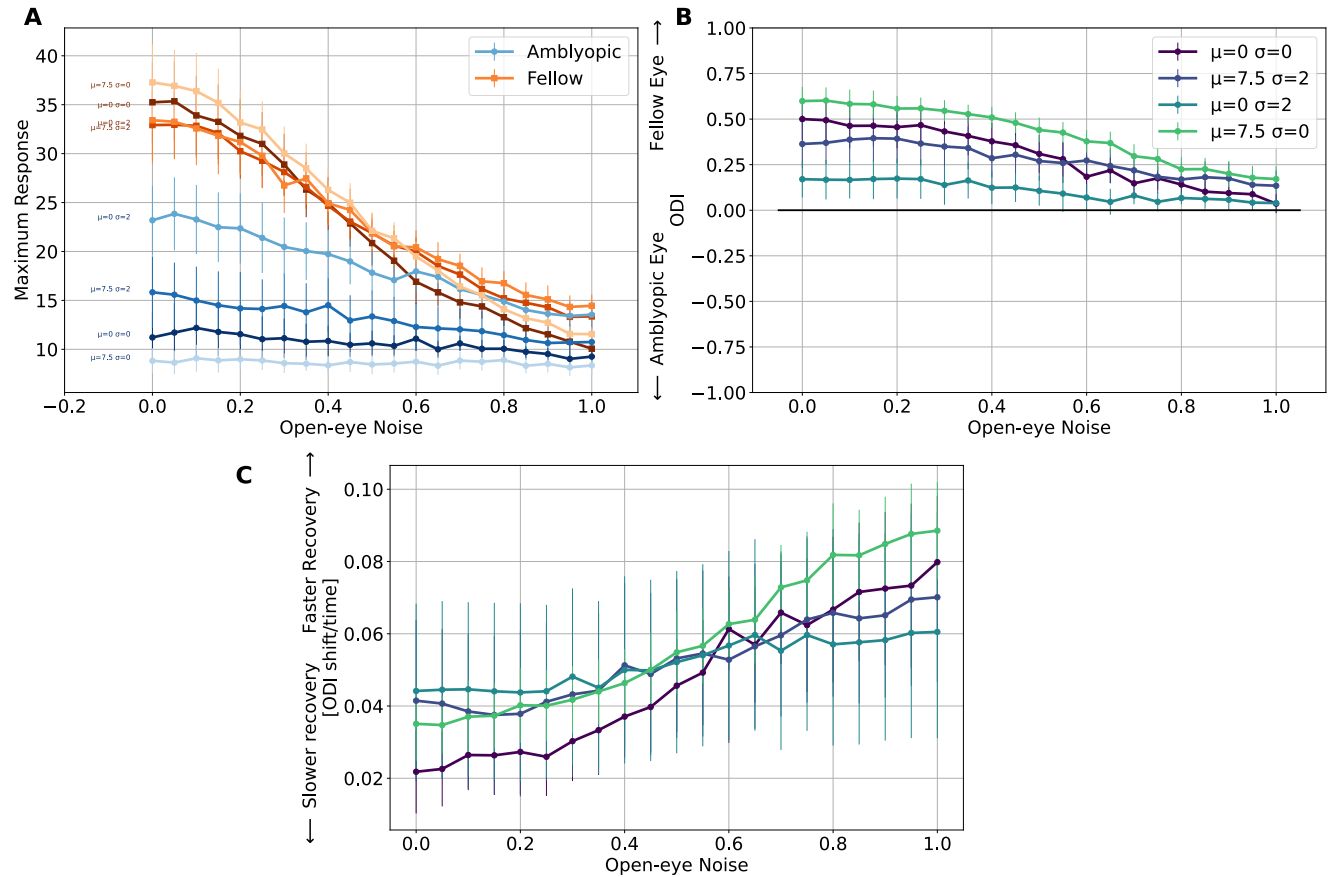


Figure 17: Optical fix treatment (A) maximum response for the amblyopic- and fellow-input channels, (B) the resulting ODI and (C) the recovery rate (i.e. ODI shift per time). Each is shown as a function of the open-eye noise with several combinations of the jitter offset mean (μ_c) standard deviation (σ_c).

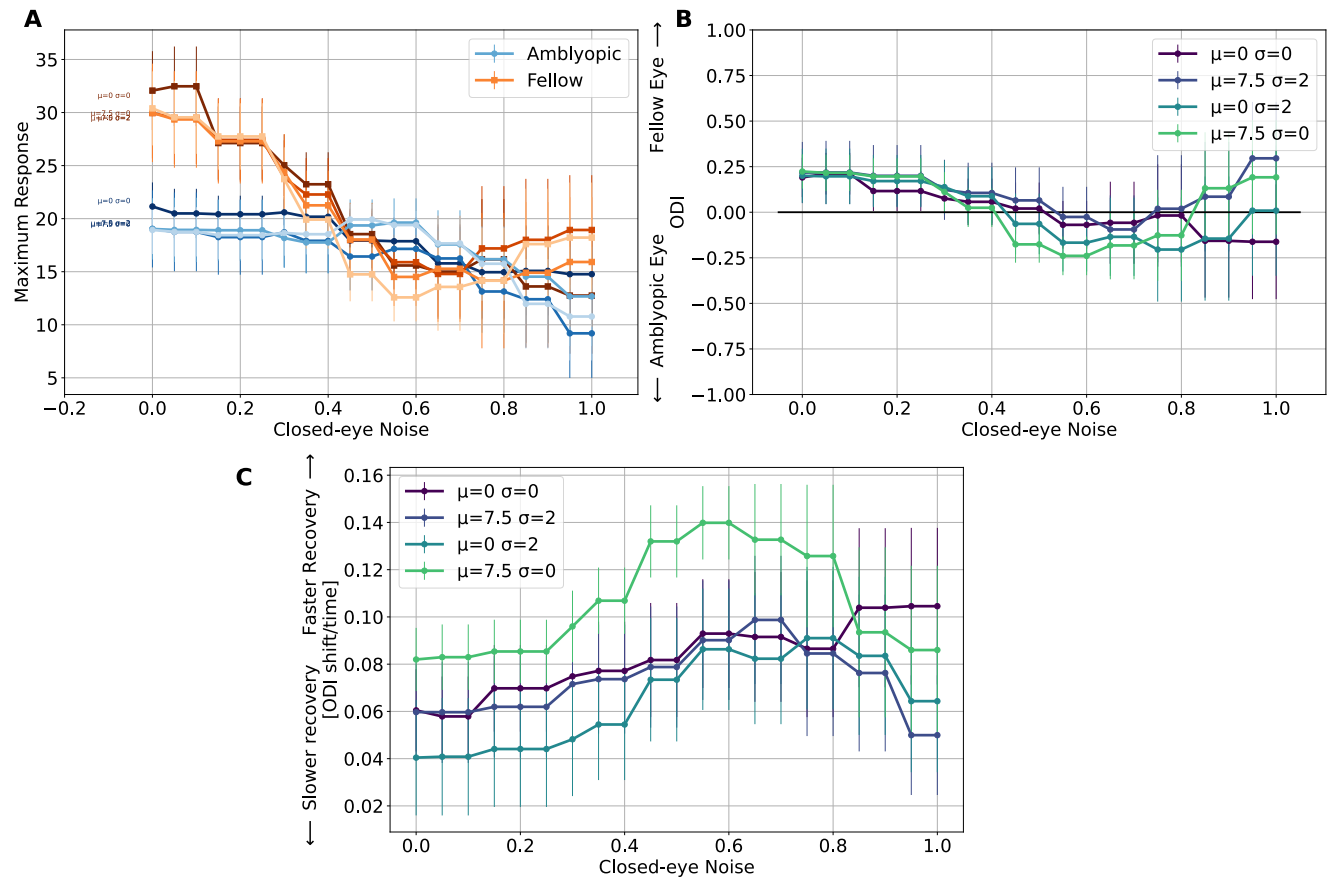


Figure 18: Patch treatment (A) maximum response for the amblyopic- and fellow-input channels, (B) the resulting ODI and (C) the recovery rate (i.e. ODI shift per time). Each is shown as a function of the open-eye noise with several combinations of the jitter offset mean (μ_c) standard deviation (σ_c).

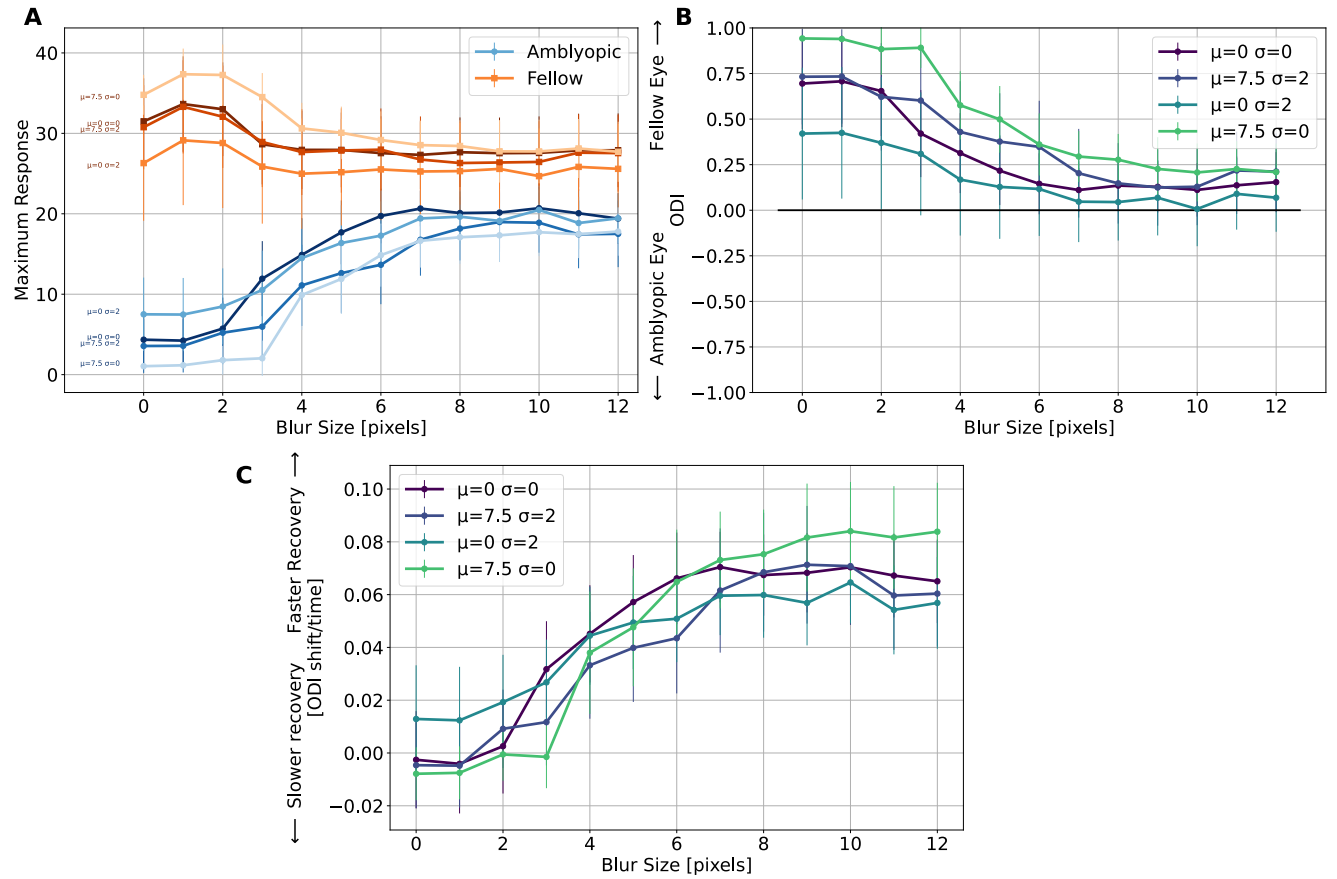


Figure 19: Atropine treatment (A) maximum response for the amblyopic- and fellow-input channels, (B) the resulting ODI and (C) the recovery rate (i.e. ODI shift per time). Each is shown as a function of the open-eye noise with several combinations of the jitter offset mean (μ_c) standard deviation (σ_c).

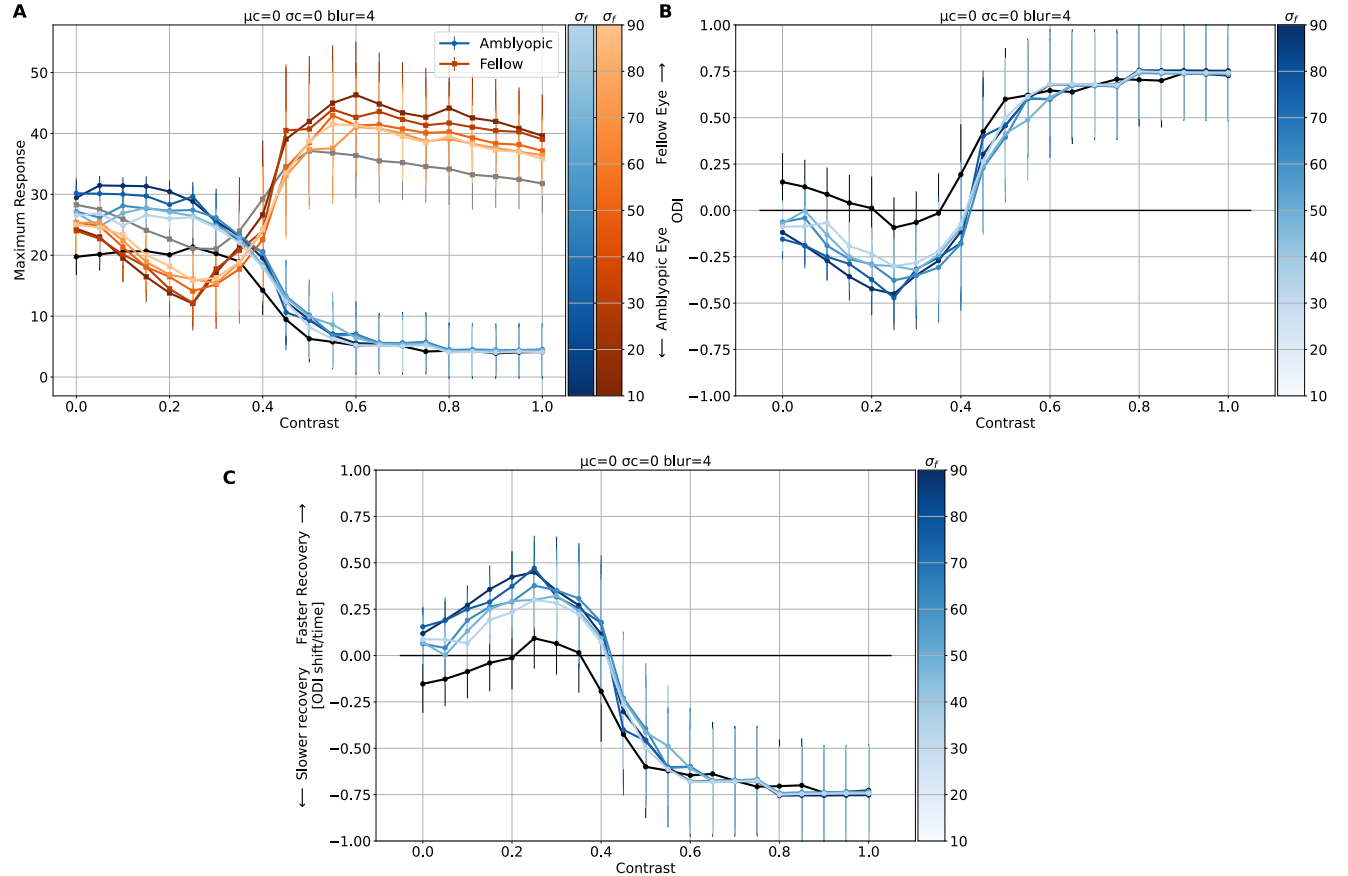


Figure 20: Dichoptic mask treatment (A) maximum response for the amblyopic- and fellow-input channels, (B) the resulting ODI and (C) the recovery rate (i.e. ODI shift per time) for the case of jitter offset mean $\mu_c = 0$ and standard deviation $\sigma_c = 0$. This is the no eye-jitter case. Each quantity is shown as a function of the contrast applied to the fellow eye. Contrast=1 means no contrast difference between the fellow- and amblyopic-eye inputs. Contrast=0 means that the fellow eye is completely silent, except for possible added noise. Shown in black is the no-mask situation. The size of the mask moves from a sharp mask with little input overlap, $\sigma_f = 10$, to a fuzzy mask with a large amount of input overlap, $\sigma_f = 90$.

affect the cases for high contrast where there is no recovery. These high-contrast cases have the fellow eye dominant.

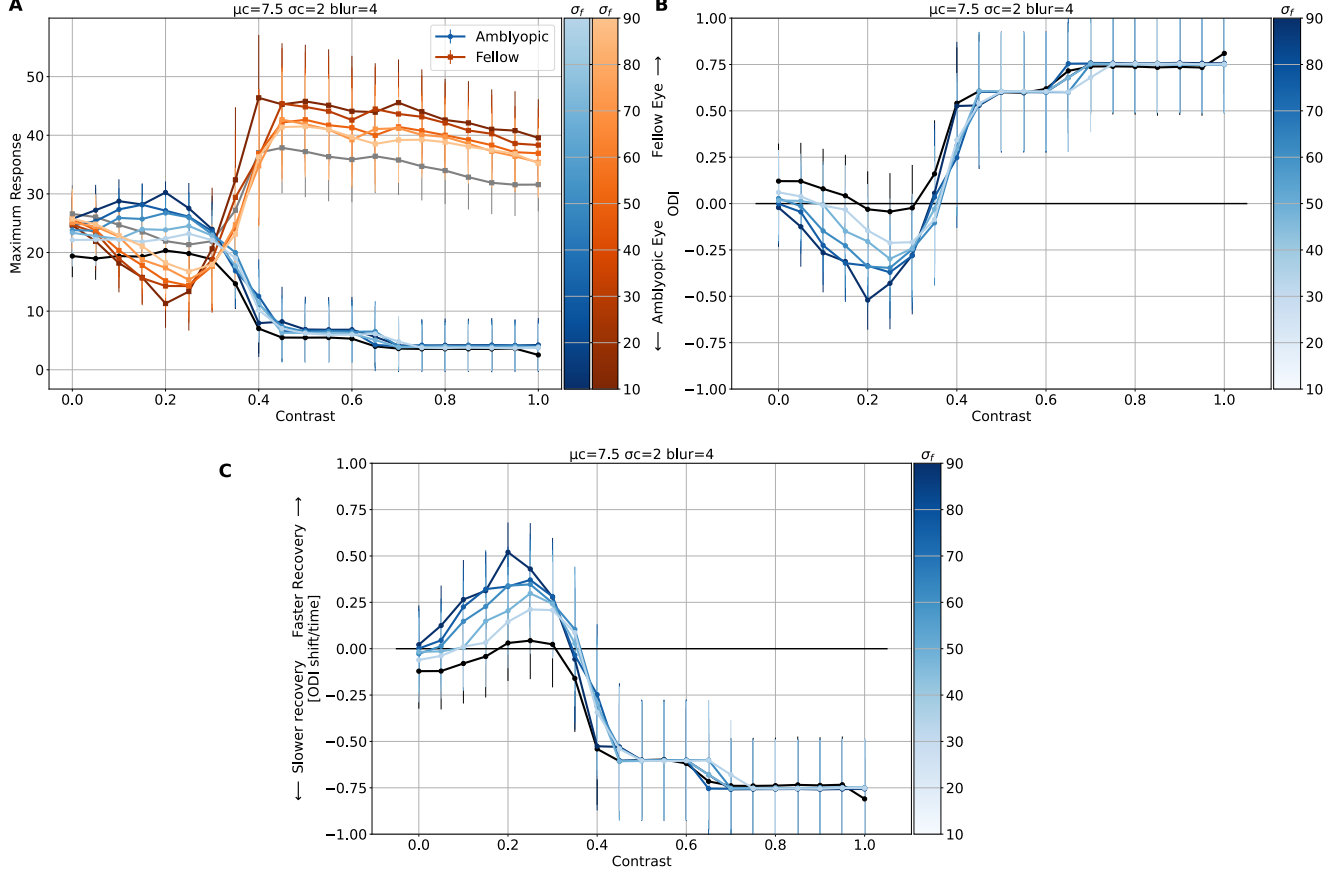


Figure 21: Dichoptic mask treatment (A) maximum response for the amblyopic- and fellow-input channels, (B) the resulting ODI and (C) the recovery rate (i.e. ODI shift per time) for the case of jitter offset mean $\mu_c = 0$ and standard deviation $\sigma_c = 0$. This is the no eye-jitter case. Each quantity is shown as a function of the contrast applied to the fellow eye. Contrast=1 means no contrast difference between the fellow- and amblyopic-eye inputs. Contrast=0 means that the fellow eye is completely silent, except for possible added noise. Shown in black is the no-mask situation. The size of the mask moves from a sharp mask with little input overlap, $\sigma_f = 10$, to a fuzzy mask with a large amount of input overlap, $\sigma_f = 90$.

Both Figure 20 and Figure 21 show a marked reverse amblyopia effect in the time-frame of the simulation – because the recovery rate is so high. It seems to be tempered somewhat with a sharper mask, but more simulations need to be run to see if the effect is statistically significant. This suggests that, in addition to increasing the contrast of the fellow eye, one could modify the mask to reduce the chance of reverse amblyopia.

4 Conclusions and Discussion

While the results of this work are promising, there are a number of limitations. This model is a single-neuron model which means it doesn't take into account any network effects, such as the balance of excitatory and inhibitory influences. It also is an early-vision model, so it does not include any object recognition, higher-order vision processes or memory processes that may be involved with amblyopia. We measure ocular dominance for convenience because

spatial frequency, which would be a more natural quantity to use for amblyopia, is too noisy for a model with 19x19 input patches. Finally, this is not a biophysical model, so neuron spike-effects are not covered.

However, the model does allow one to run many different scenarios with as few assumptions as possible. It can capture the dynamics of the learning in the visual system in these scenarios, and allows us to explore the benefits and drawbacks of different treatment paradigms.

Given that both the contrast of the fellow eye and the dichoptic mask influence the rate of recovery, one could modify the mask or the contrast to reduce the chance of reverse amblyopia. One would want frequent measurements of the inter-eye imbalance to recognize when such a change is warranted.

Some lingering questions

Here are just a couple of things I noticed, that I need to look into to see if there are any issues.

- I would have expected a reverse amblyopia effect with the patch treatment, but I don't see that. It might be washed out in the variation at high noise level, but I want to be sure
- I would have expected that in the dichoptic treatment, that the case of contrast=1 with no mask would be identical to the optical fix at an open-eye noise level of 0.1. I don't see that, so I am not sure what the difference is
- I think it would be useful to run a couple of these cases for more systematic changes in the jitter mean and standard deviation. There wasn't much of an effect, but it is there in places and it would be easier to communicate this with a few examples

References

- Bienenstock, E. L., Cooper, L. N., and Munro, P. W. (1982). Theory for the development of neuron selectivity: Orientation specificity and binocular interaction in visual cortex. *Journal of Neuroscience*, 2, 32–48.
- Birch, E. E. (2013). Amblyopia and binocular vision. *Progress in Retinal and Eye Research*, 33, 67–84.
- Blais, Brian S. (1998, May). *The role of the environment in synaptic plasticity: towards an understanding of learning and memory* (PhD thesis). Brown University, Institute for Brain; Neural Systems; Dr. Leon N Cooper, Thesis Supervisor.
- Blais, Brian S., Frenkel, M. Y., Kuindersma, S. R., Muhammad, R., Shouval, H. Z., Cooper, L. N., and Bear, M. F. (2008). [Recovery from monocular deprivation using binocular deprivation](#). *J Neurophysiol*, 100(4), 2217–24.
- Blais, B. S., Intrator, N., Shouval, H., and Cooper, L. N. (1998). Receptive field formation in natural scene environments: Comparison of single cell learning rules. *Neural Computation*, 10(7), 1797–1813.
- Carandini, M., and Heeger, D. J. (2012). Normalization as a canonical neural computation. *Nature Reviews Neuroscience*, 13(1), 51–62.
- Charters, L., and Ghasia, F. (2022). Unraveling the mysteries of amblyopia and fixation eye movements. *Ophthalm-*

- mology Times*, 47(4).
- DeAngelis, G. C., Ohzawa, I., and Freeman, R. D. (1995). Receptive-field dynamics in the central visual pathways. *Trends in Neurosciences*, 18(10), 451–458.
- Gao, T. Y., Guo, C. X., Babu, R. J., Black, J. M., Bobier, W. R., Chakraborty, A., et al., et. (2018). Effectiveness of a binocular video game vs placebo video game for improving visual functions in older children, teenagers, and adults with amblyopia. *JAMA Ophthalmology*, 136(2), 172.
- Glaser, S. R., Matazinski, A. M., Sclar, D. M., Sala, N. A., Vroman, C. M., Tanner, C. E., et al.others. (2002). A randomized trial of atropine vs patching for treatment of moderate amblyopia in children. *Archives of Ophthalmology*, 120(3), 268–278.
- Hess, R. F., and Thompson, B. (2015). Amblyopia and the binocular approach to its therapy. *Vision Research*, 114, 4–16.
- Holmes, Jonathan M., Manh, V. M., Lazar, E. L., Beck, R. W., Birch, E. E., Kraker, R. T., et al., et. (2016a). Effect of a binocular iPad game vs part-time patching in children aged 5 to 12 years with amblyopia. *JAMA Ophthalmology*, 134(12), 1391.
- Holmes, Jonathan M., Manh, V. M., Lazar, E. L., Beck, R. W., Birch, E. E., Kraker, R. T., et al.others. (2016b). A randomized trial of a binocular iPad game versus part-time patching in children 5 to 12 years of age with amblyopia. *JAMA Ophthalmology*, 134(12), 1391.
- Kelly, K. R., Jost, R. M., Dao, L., Beauchamp, C. L., Leffler, J. N., and Birch, E. E. (2016). Binocular iPad game vs patching for treatment of amblyopia in children. *JAMA Ophthalmology*, 134(12), 1402.
- Li, S. L., Reynaud, A., Hess, R. F., Wang, Y.-Z., Jost, R. M., Morale, S. E., et al. Birch, E. E. (2015). Dichoptic movie viewing treats childhood amblyopia. *J AAPOS*, 19(5), 401–5.
- Ruderman, D. L., and Bialek, W. (1994). Statistics of natural images: Scaling in the woods. *Physical Review Letters*, 73(6), 814.
- Wallace, D. K., Repka, M. X., Lee, K. A., Melia, M., Christiansen, S. P., Morse, C. L., and Sprunger, D. T. (2018). Amblyopia preferred practice pattern®. *Ophthalmology*, 125(1), P105–P142.
- Xiao, S., Angjeli, E., Wu, H. C., Gaier, E. D., Gomez, S., Travers, D. A., et al.others. (2022). Randomized controlled trial of a dichoptic digital therapeutic for amblyopia. *Ophthalmology*, 129(1), 77–85.
- Xiao, S., Gaier, E. D., Mazow, M. L., Stout, A. U., Travers, D. A., Angjeli, E., et al. Hunter, D. G. (2020). Improved adherence and treatment outcomes with an engaging, personalized digital therapeutic in amblyopia. *Scientific Reports*, 10(1), 1–8.
- Zárate, B. R. de, and Tejedor, J. (2007). Current concepts in the management of amblyopia. *Clinical Ophthalmology (Auckland, NZ)*, 1(4), 403.